Journal of Physics: Conference Series

Modeling of destructive interaction of hot jet and solid plate

Journal of Physics: Conference Series **1787** (2021) 012062 doi:10.1088/1742-6596/1787/1/012062

Modeling of destructive interaction of hot jet and solid plate

T M Muruganandam[1], E E Son[2], M Kh Gadzhiev[3] and S P Vetchinin[3]

[1] Indian Institute of Technology Madras, 1st Cross Road, Chennai, Tamil Nadu 600036, India
[2] Moscow Institute of Physics and Technology, Institutskiy Pereulok 9, Dolgoprudny, Moscow Region 141701, Russia
[3] Joint Institute for High Temperatures of the Russian Academy of Sciences, Izhorskaya 13 Bldg 2, Moscow 125412, Russia

E-mail: makhach@mail.ru

Abstract. Based upon the results of a literature review, a set of physical parameters suitable for quantitative comparison in experimental and numerical studies is determined. The review showed the feasibility of modeling the process of the outflow of an immersed jet of inert gas into the surrounding space and the evolution of a free shear layer formed by hot and cold gases to analyze the process of convective and diffusion transport of various types of particles. In the model formulation we consider the problem of solid destruction by a melt of the same substance, as well as by a nitrogen stream at high temperature. The test simulation of the problems of two-phase interaction of a immersed jet of molten liquid and hot gas, on the whole, qualitatively showed the reproduction of the main characteristics of the flow: the generation of large-scale vortices around the jet in the induction zone, the oscillations of the jet when it collides with an obstacle, and the shape of the cavity formed.

1. Introduction

Low-temperature plasma (LTP) generators create a stream of highly ionized quasineutral gas, which in some cases forms a jet immersed into the surrounding space allowing regarding this process as a classical problem of fluid mechanics. The fluid jet is an unstable unsteady flow that has several evolution stages on a scale determined by the characteristic size—the diameter of the outlet D (or width W in planar case). Accordingly, one can introduce the characteristic Reynolds number $\mathrm{Re_D} = \rho U D/\mu$ at this scale, where U to be the characteristic speed, ρ to be the density, μ to be dynamic viscosity. A submerged jet appears to be extremely sensitive to perturbations of velocity and pressure emerged from the nozzle exit region. Artificially generated disturbances (using vibrating plates, acoustic speakers, auxiliary inlet channels) can be axial or spiral, and their amplitude can be about 0.01% of the speed U [1]. Such excitations allow to control mixing intensity and, in some cases, to divide the turbulent jet into two or three streams with a maximum divergence angle of 160°. The nature of the flow instability is also determined by perturbations propagating through the gas duct of the gas-dynamic facility (LTP generator), nozzle block eigenfrequencies, hydrodynamic perturbations from stationary vortices at gas path elbows, and the boundary layer break-up at sharp edges.

Along with the nozzle exit section a free shear layer is an important element of the submerged jet too. Its properties, such as an average velocity $\bar{U}$, velocity difference ΔU, the maximum shear $|\partial U/\partial y|_{\max}$ [2], the size of the initial displacement or momentum thickness to a large extent determine the instability mode (convective or absolute [3]), as well as its increment. The growth of instability in the shear layer is intrinsically two-dimensional at least at the linear stage of evolution [4]. Further development leads to the roll-up of Kelvin–Helmholtz vortices, which in the case of a three-dimensional jet have a toroidal shape. Their intensity determines the entrainment rate of surrounding fluid in the jet and the destruction of the core, the shape of resulting coherent structures in the far field of the stream.

The immersed jet is divided into several sections (at least three): the initial section ($z/D \lesssim 6$), transitional section ($6 \lesssim z/D \lesssim 20$), and the main one (self-similar, $z/D \gtrsim 20$), where z to be a distance from the outlet. An important parameter is the characteristic Mach number M in the boundary layer, which determines the effect of compressibility [2].

The described scenario of evolution will be significantly complicated if jet is composed of thermal plasma. A large gap across the shear in a number of thermodynamic quantities (density, temperature, etc) should have a significant effect on the instability development, as well as on the of mixing with host fluid.

An important factor is plasma radiative quenching due to nonequilibrium radiation, which leads to the rapid cooling of macroscopic fluid parcels and decrease in their volume, as well as the equilibrium recombination of atoms and molecules that change, in particular, the average molar mass of the mixture. Observing the mixing process and the resulting structures in a recombining plasma jet, as well as finding the velocity distribution, is a difficult task due to high temperatures leading to the evaporation of tracer particles and the destruction of measuring probes, and the high luminescence intensity of gases leaving the plasma torch.

This article is structured in the following way. In section 2, we provide a brief overview of effective experimental diagnostics providing independent measurements of velocity, temperature and concentrations of species. These methods allow obtaining profound and reliable data to be compared with numerical investigations. The latter appears to be rather difficult task as plasma jet evolution is accompanied by shear flow instabilities, developed turbulence and huge chemical and heat diffusion rates. We finalize section 2 depicting our results on graphite ablation visualized by laser knife. In section 3, we build two models of jet-solid destructive interaction departing from classical Stefan problem. The first models deals with the interaction of the immersed tin jet with solid plate of the same substance. In the second model, we move from liquid tin to gaseous nitrogen stream, trying to achieve heat fluxes and to maintain algorithm stability.

2. Convective and molecular transport in the immersed jet of thermal plasma

In addition to well-known methods for measuring plasma velocity and temperature, such as Pilot's tube, tracing particles seeded into plasma, spectroscopic measurements of spontaneous emission of excited species, immersed plasma jets are experimentally investigated using Thomson scattering, 2-photon induced laser fluorescence, enthalpy probes, coherent anti-Stokes Raman spectroscopy.

These methods provide a fairly complete picture of hydrodynamic and thermal characteristics, as well as determine the concentration of some species. In particular:

- enthalpy probe measures total oxygen concentration, velocity and temperature profiles in the flow;
- Thomson scattering—a non-invasive method allowing independent measurements of plasma velocity and temperature, which can be compared with the data of an enthalpy probe;

- using fluorescence induced by a 2-photon laser it is possible to determine the concentration of atomic oxygen;
- molecular oxygen concentration and temperature are measured using coherent anti-Stokes recombination scattering spectroscopy;
- the schlieren method determines the ratio of the densities in the jet and the surrounding gas visualizing vortex zones.

The indicated approaches were used elsewhere [5] for the experimental study of a argon jet from an industrial plasma torch with characteristic plasma temperature $T = 12\,000$ K, ionization degree $\alpha_{\mathrm{i}} \approx 0.1$–$0.3$, velocity over 1000 m/s, Mach number $\mathrm{M} \approx 0.5$. Since such plasma torches are often used for plasma spraying, the measurements of macroscopic mixing and molecular diffusion rates of atmospheric gases into the jet and their subsequent reaction with particles of the sprayed powder are extremely important. Due to high temperatures the differences in a material parameters and transport coefficients, particularly in density, remain in the far field of the jet, even though the jet quickly dissipates due to capture of the surrounding fluid. The entrainment changes the chemical composition and quickly slows down and cools the jet, creating an oxidizing atmosphere and changing the efficiency of melting and particle acceleration.

Using the schlieren method, it was found that the mixing of the jet with the surrounding liquid is turbulent. Indeed, according to [6], if the characteristic Reynolds number (by mass average values) exceeds 400, the shear layer at the exit of the plasma torch is turbulent either. The accelerated turbulization of the mixing layer is possibly preceded by the turbulization of a sufficiently thick boundary layer on the inner surface of the gas duct of the plasma torch, which has a relatively low temperature. However, due to the high temperature, low density, and relatively high viscosity at the jet centerline, the core remains laminar at the outlet.

At the initial section of the jet the process of vorticity generation in the irrotational fluid is kinematic (determined by the Biot–Savart law), and such fluid particles immediately adjacent to the shear layer, begin to participate in large-scale shear movements long before they acquire their own vorticity through diffusion.

For large Reynolds numbers dimensional considerations [6] allow to obtain an expression for the time required to achieve the determination of a certain size of the vortex (the required wave number k, or spatial scale) [7]. The time to reach the Kolmogorov scale is $\tau_{\lambda_0} \approx 2k_1\delta/U$, where δ to be the thickness of the shear layer, and k_1 to be a constant of the order of unity.

The concentration diffusion time in a vortex of the size λ is $\tau_{\lambda_{\mathrm{d}}} \approx \lambda^2/d$, and the propagation time of the heat wave is $\tau_{\lambda_\alpha} \approx \lambda^2/\alpha$, where d to be the diffusion coefficient and α to be the thermal diffusivity. The Damköhler number is the ratio of the time scales of mixing (or diffusion) and the chemical reaction, and for large scales it has the form $\tau_{\lambda_0}/\tau_{\mathrm{c}}$, and diffusion at small scales [8] to be $\tau_{\lambda_{\mathrm{d}}}/\tau_{\mathrm{c}}$ and $\tau_{\lambda_\alpha}/\tau_{\mathrm{c}}$, respectively, where τ_{c} to be the characteristic reaction time.

Large Damköhler numbers show that the mixing process is limited by chemical reactions, while small values indicate the limited occurrence of chemical reactions.

The characteristic diffusion scale λ_{D} differs from the Kolmogorov scale by the reciprocal of the Schmidt number [9], $\lambda_{\mathrm{d}} = \lambda_0 \mathrm{Sc}^{-1/2}$. Similarly, for heat transfer, we have the relation $\lambda_\alpha = \lambda_0 \mathrm{Pr}^{-1/2}$, where Pr to be the Prandtl number. In gases $\mathrm{Pr} \approx \mathrm{Sc} \approx 1$, therefore, at the Kolmogorov scale, diffusion plays a dominant role. Due to the very large temperature gradients present in the high-temperature jets, significant heat transfer at the boundaries of cold induced vortices can occur before the mixing of fluid particles takes place at the Kolmogorov scale. This fact makes the intermediate stage of mixing crucially important.

Thus, in the case of air (containing nitrogen and oxygen) entrainment by a high-temperature jet, dissociation of a significant amount of trapped gas can take place over a time much shorter than the time to reach complete equilibrium at small scales. For high-temperature plasma jets, density effects are also important [6]. Accelerated mixing and entrainment in low-density jets

followed by mixing of shear layers was also observed in [10–12]. A density ratio below 0.72 leads to the development of a specific jet instability [13, 14], which is associated with the formation of large unsteady axisymmetric vortex structures that rapidly increase host fluid entrainment.

The instabilities, which occur in the jet, are also dependent upon fluctuations in the supply voltage and the characteristics of the arc. These oscillations lead to the formation of large-scale perturbations with a characteristic scale of the order of the jet initial radius. The flow characteristics at the nozzle exit, as well as the properties of the growing boundary layer in the plasma torch channel, strongly affect the jet evolution [15], which inhibits comparing the results of experiments obtained by various authors.

An important and probably still unresolved issue is the form of the invariants along the streamline in a view of plasma quenching. Based on the model of an incompressible fluid, the use of Bernoulli-type invariants is sometimes proposed.

In the range of Mach numbers, at which compressibility effects are important, it is assumed that the flow is decelerated isentropically with a frozen plasma composition [16].

The smallest (Kolmogorov) scale of the vortices in the transition section of the plasma jet is estimated [17] as $\lambda_0 = \delta \mathrm{Re}^{3/4}$ and is about 0.1 mm. However, this scale is somewhat smaller than the results of the Schlieren method (0.5 mm) [5]. The mixing time on the Kolmogorov scale is of the order of $\tau_{\lambda_0} = \delta/\Delta v = 40$ μs. The characteristic propagation time of the heat wave $\tau_{\lambda_\alpha} = \lambda^2/\alpha$ is about 50 μs. Consequently, the time to reach the smallest scales and the time required to establish thermal equilibrium are of the same order of magnitude. Cold ambient air, which is continuously entrained into the stream and carried downstream, can survive for tens of millimeters in the vortex cascade and when the temperature is equalized. The corresponding Damköhler number is $\tau_{\lambda_\alpha}/\tau_d = 10$.

The recombination process in a jet [5] occurs at a relatively low temperature, of the order of 2000 K. At this temperature, the time constant for recombination is of the order of 1 ms, which indicates a greater effect on the reaction rate. It was found that both on the jet axis at $z/D > 8$ and in the mixing layers, the concentration of atomic oxygen exceeds equilibrium values. Fincke et al. [5] noted that although cold vortices can survive for long periods of time, the hot ones have a shorter characteristic equilibrium time of about 10 μs, which leads to a Damköhler number of about 0.01, indicating the importance of the recombination rate.

Experiments show that in a plasma jet there are significant deviations from equilibrium and that mixing to a molecular level is incomplete in a significant part of the flow. This important feature is associated with incomplete mixing, as well as with the recombination rate during expansion and cooling of the jet.

A review of the literature shows the feasibility of modeling the process of the outflow of a jet of inert gas into the surrounding space, due to the possibility of quantitative comparison with experimental results. It is also necessary to simulate a free shear layer formed by hot and cold gases to analyze the process of convective and diffusion transport of various types of particles. Available experimental data allow us to expand the set of parameters for quantitative comparison with the results of numerical studies—in addition to speed, pressure, temperature and heat flux, one can use density, as well as the concentration of individual types of particles.

In [18–23], we were studying the process of graphite sublimation in a chemically active and inert plasma created by LTP generator with an expanding channel of the output electrode having a number of technological advantages [24].

The important information on plasma properties in its head flow on the sample can be provided by video recording and stereo imaging of the cavity formation zone. Graphite particles heated by a high enthalpy flow leave tracks on the video frames. Being small enough, they move in phase with the plasma jet and the particle velocity can be estimated via the exposure time and the track length [figure 1(a)]. Rectangular (parallelepipeds of sides 12–25 mm and a thickness of 3.5 and 7 mm) and cylindrical (diameter of 20 mm, thickness of 2, 4 and 6 mm) samples were

(a) (b)

Figure 1. (a) Carbon sample with nitrogen plasma jet and sublimate puffs. (b) Sample shape during sublimation under argon plasma jet, the profile of the resulting cavity is visualized using a green laser knife.

made of isotropic and anisotropic graphite. In nitrogen plasma when reaching a sample surface temperature of 2500 K, optically semi-opaque puffs were observed. These sublimated carbon fines aggregations change their shape and size driven by plasma flow. The characteristic time of interaction of a plasma jet with enthalpy of about 20 kJ/g is sufficient for sublimation of half the initial mass of a sample weighing about 2 g (1 cm^3) in 30–40 s at a distance from the nozzle exit of $Z_0 = 20$ mm and arc current 250 A.

Further heating of the sample surface in nitrogen plasma leads to periodic bursts of graphite particles moving at a speed of 30–100 m/s. The process of intense graphite sublimation lasts 20–30 s and then continues in steady state when the sample reaches temperature at which radiative losses compensate the heat influx from the plasma jet.

The maximum temperature is 4200 ± 200 K for a cylindrical sample and 4000 ± 200 K for the rectangular one. Resting upon the obtained temperature fields one can conclude that the maximum sample temperature is of the order of 3600–4200 K. In case of chemically inert argon plasma jet centerline temperature reaches 2500 K in a short time (5–6 s), and the sample outside the crater [figure 1(b)] is heated by thermal diffusion up to 2000 K, that also leads to the onset of sublimation from a heated surface.

Although the ablation process was studied on a graphite target, the tin destruction will be simulated in the next section due to several methodological reasons (liquid graphite does not exist), and also because of high ablation enthalpy (an order of magnitude greater compared to tin), which increases problem computing size significantly.

3. Simulation of immersed jet melting a solid body

The starting point of this study is the test problem of solidification of pure tin in the presence of overheating of the liquid (Stefan's problem) [25, 26] in a rectangular region with vertical boundaries having different temperatures. This temperature variation is significantly less than tin melting temperature $T_\mathrm{m} = 505$ K. When simulating this two-phase problem COMSOL Multiphysics computational algorithm is robust and provides correct solution.

Based on the results for two-phase convection, we consider a model of a jet of incompressible liquid colliding with a solid surface of the same substance. As in [25], we assume that the

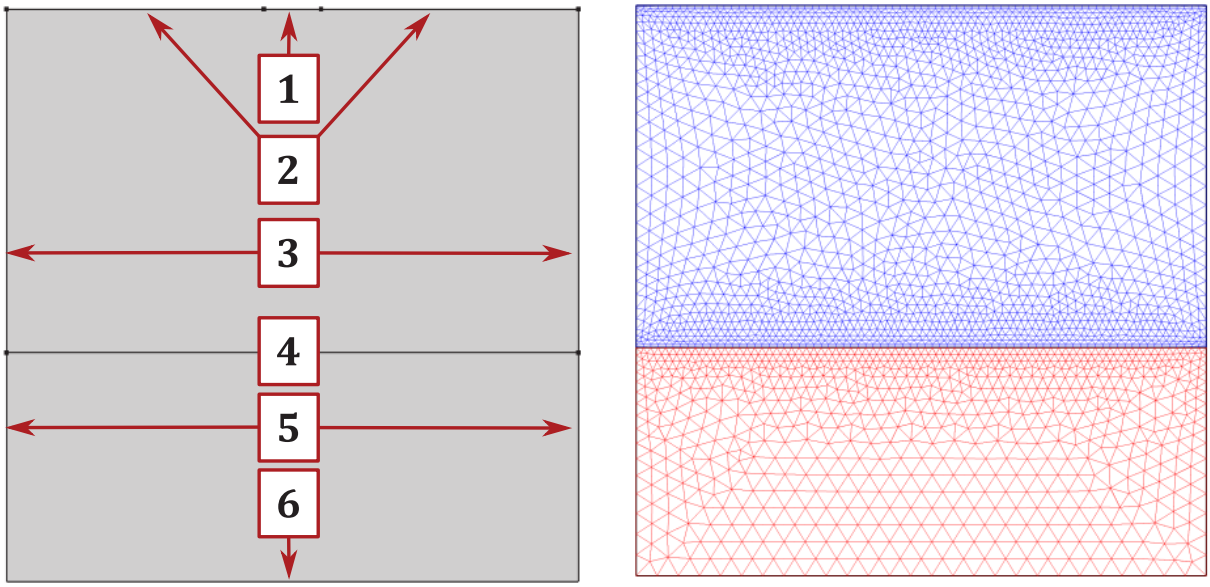

Figure 2. (a) Computational domain: 1—jet inlet interval; 2—upper boundary; 3—boundaries of the liquid phase; 4—movable horizontal boundary; 5—vertical boundaries; 6—bottom boundary. (b) Deformable mesh, the up side (blue) corresponds to the liquid region, the down side (red) corresponds to the solid material region.

thermophysical properties of tin in the liquid and solid states are temperature independent, the melt is a Newtonian liquid, and we also neglect the finite values of the velocities at the interphase boundary due to a change in volume during melting. The calculation is carried out in a two-dimensional rectangular domain 0.1×0.1 m^2 in size.

At the upper boundary, along with jet inlet interval, a constant temperature $T_1 = 508$ K is set [figure 2(a)]. The width of a plane inlet is 1 cm. At the left and right boundaries of the domain corresponding to liquid phase, the conditions for free flow and zero heat flux are set. The movable vertical boundary corresponds to the melting temperature of 505 K, and can shift downward if the heat flux carried by immersed jet is able to warm the solid boundary up to the melting temperature. The shift of the moving boundary in the calculation leads to deformation of the computational grid, which consists of two regions corresponding to the liquid and solid phases [figure 2(b)]. At the vertical boundaries, conditions of zero heat flux are set.

At the bottom boundary below the melting region temperature has the value $T_2 = 503$ K.

Figure 2(b) shows a characteristic view of computational grid formed by triangular elements refined at horizontal boundaries, as well as at the melting zone. The boundary between meshes constructed for liquid and solid phases changes its position according to

$$\rho_{\mathrm{Sn}} q_{\mathrm{Sn}} \frac{\mathrm{d}\boldsymbol{x}}{\mathrm{d}t} \cdot \boldsymbol{n} = (\boldsymbol{F}_{\mathrm{in}} - \boldsymbol{F}_{\mathrm{out}}) \cdot \boldsymbol{n}, \tag{1}$$

where ρ_{Sn} to be the tin density (kg/m^3), q_{Sn} to be tin specific fusion heat (J/kg), $\boldsymbol{F}_{\mathrm{in}}$ to be the heat flux from liquid phase to the interface, $\boldsymbol{F}_{\mathrm{out}}$ to be the heat flux from solid phase.

The boundary conditions should be set with precautions as in the case of steep gradients the initial stage of jet motion (when the layers of the surrounding fluid begin to move) can be calculated with an extremely small spatial step or will not converge at all. This problem can be solved using built-in step functions. Our experience shows that decaying exponential

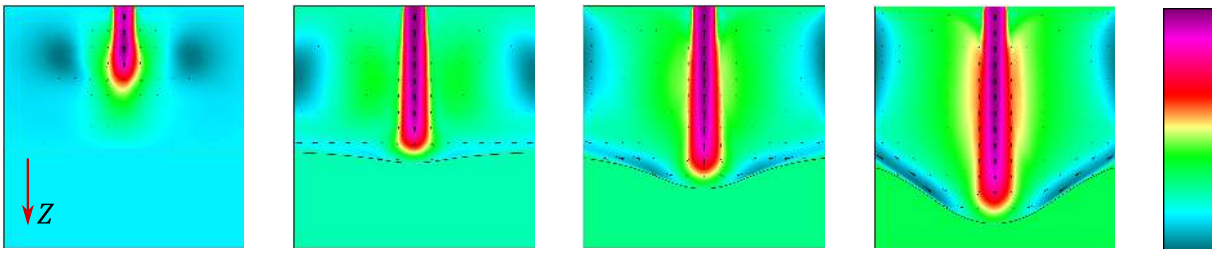

Figure 3. The color field of the heat flux along Z-axis as well as the heat flux vector at different moments and the corresponding color scale ranges (W/m^2): (a) 2 s, $[-1.47 \times 10^7, 4.72 \times 10^7]$; (b) 6 s, $[-1.38 \times 10^7, 4.74 \times 10^7]$; (c) 15 s, $[-1.8 \times 10^7, 4.87 \times 10^7]$; (d) 30 s, $[-2.43 \times 10^7, 5.02 \times 10^7]$.

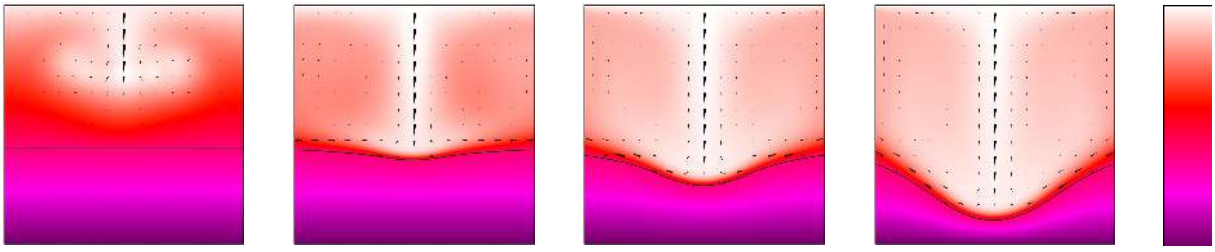

Figure 4. The color field (from violet to white) shows temperature T distribution. The vectors show the direction of spreading liquid. The scale is in the range from 503 to 508 K. The physical time of the process: (a) 2, (b) 6, (c) 15, (d) 30 s.

functions $F(t) = 1 - \exp(-at)$ where a to be some arbitrary coefficient and t to be a physical time can also be adopted. For a jet the condition for the mass fluid flow is specified in the form $Q_\mathrm{m} = a[1 - \exp(-t)]$, where $a = 0.9$ kg/s and t to be dimensionless time, which ensures algorithm stability in the transition mode. The total number of grid cells is 5203.

Figure 3 shows the distribution of the heat flux in the vertical direction at different time instants indicating very large heat fluxes up to 50 MW/m^2 at relatively low speeds (about 0.15 m/s). The development of a flow in a liquid region is associated with the formation of two vortices as the submerged jet moves to a solid surface, which then increase in size and have a rounded core. The onset of melting ($t \approx 5$ s) leads to deformation of the vortex zone. Impinging fluid flow forms a stagnant region at the collision point and also begins to spread over the solid surface. The cavity deepening ($t \approx 15$–20 s) leads to separation of streams of spreading fluid from a solid surface. Temperature distribution in figure 4 shows that the region of maximum temperature coincides with the stagnant zone and the section of the most rapid melting. The boundary between the liquid and solid phases occupies its asymptotic position when establishing the equality of heat fluxes arriving at the grid cell from jet and the bottom cold boundary. Thus, the melting process is modeled by the displacement of the interphase boundary, which leads to a displacement of the faces of the computational grid downward, cells stretching and a general size increase of the molten tin region.

In further, we will consider modeling of a hot gas (with properties of nitrogen) impinging a tin solid plate in order to achieve heat fluxes affecting an obstacle comparable to the results of

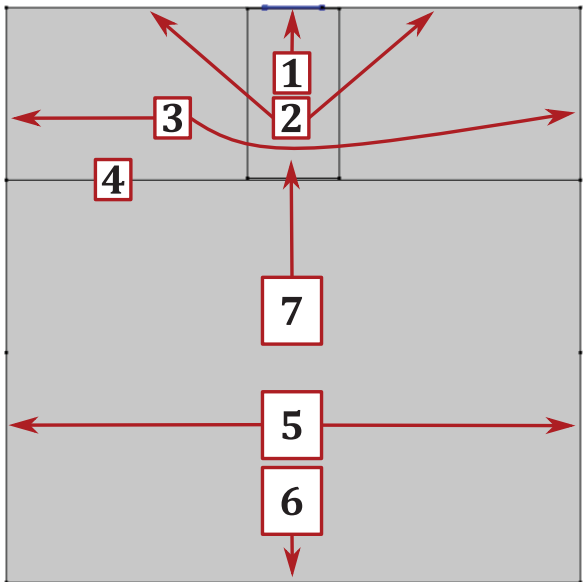

Figure 5. Modified computational domain: 1—jet inlet interval; 2—upper boundary; 3—boundaries of the liquid phase; 4—interfacial boundary; 5—vertical boundaries; 6—bottom boundary; 7—vicinity of the inlet.

the first problem. To ensure the correctness and cost-effectiveness of the calculation, a number of boundary conditions were modified (figure 5).

In particular, the impermeability condition at the upper boundary has been replaced by the free outlet to simplify the flow pattern around the jet. The latter will restrict the intensity of large-scale vortices above the solid surface, and also prevent the appearance of hot gas regions at the upper boundary of the domain in figure 5 leading to temporal step refinement. The condition for achieving melting temperature at the interfacial boundary for the mesh displacement is replaced by a system of ratios:

$$\frac{\mathrm{d}\boldsymbol{x}}{\mathrm{d}t} \cdot \boldsymbol{n} = v_\mathrm{n}, \tag{2}$$

$$v_n = \frac{T_\mathrm{lm}}{\rho_\mathrm{s} H_\mathrm{abl}}, \tag{3}$$

where $\boldsymbol{n}$ to be the normal to the cell boundary, v_n to be the speed of the boundary in the normal direction, T_lm to be the Lagrange multiplier that numerically coincides with the value of the resulting heat flux at the cell boundary, ρ_s to be the density, H_abl to be the enthalpy of ablation of the substance in the solid phase. Thus, if the heat flux from the immersed jet exceeds a certain critical value, the boundaries of the moving cells are shifted to the corresponding value.

For immersed jet mass flow $Q_\mathrm{m} = b[1 - \exp(-0.5t)]$ and temperature $T_\mathrm{j} = c + d[1 - \exp(-t)]$, where $b = 0.1$ kg/s, $c = 505$ K, $d = 5000$ K, conditions acting as limiters of spatial and temporal velocity and temperature gradients are set when establishing the flow. In the approximation used the temperature is constant over the jet cross section, while its time dependence shows that gas heating in the plasma torch does not occur immediately. Obviously, simulated derivatives $\mathrm{d}Q_\mathrm{m}/\mathrm{d}t$ and $\mathrm{d}T_\mathrm{j}/\mathrm{d}t$ are significantly less than the real values in the plasma torch. However, the calculation of these transient phenomena would require considerable processor time.

The rectangular area in the immediate vicinity of the entrance indicates the adaptation zone of the computational grid in order to improve the accuracy of the calculations. The total number of cells of the computational grid was 14 127.

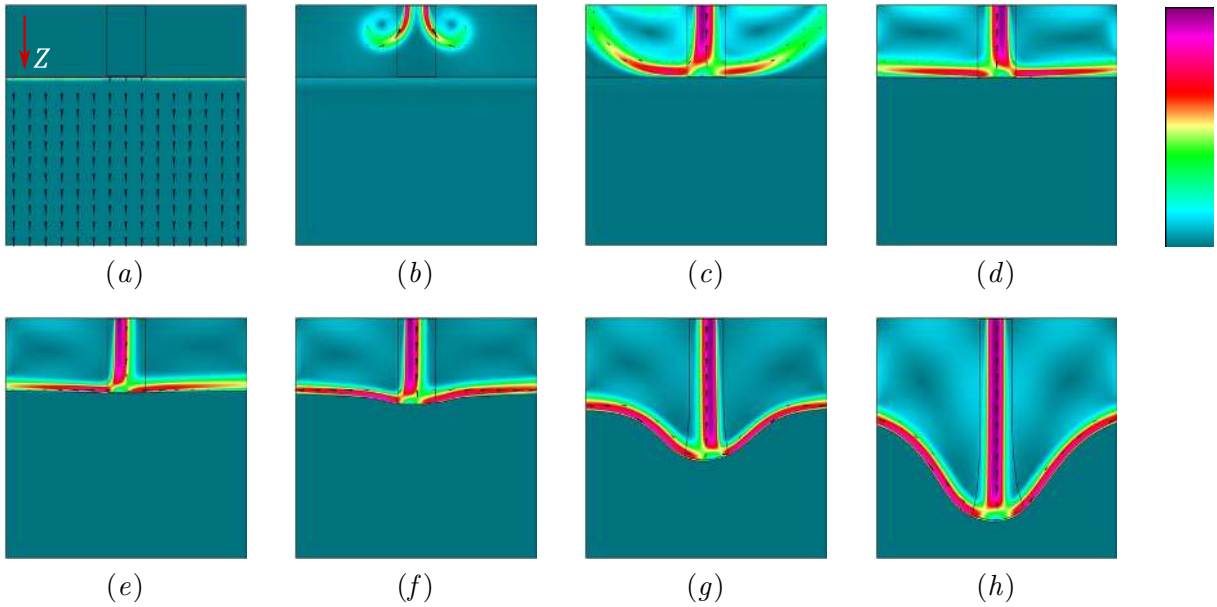

Figure 6. The distribution of heat flux in Z-axis direction at different moments with the color scale ranges (W/m^2) as follows: (a) 0 s, $[2.7 \times 10^{-3}, 2.79 \times 10^5]$; (b) 0.1 s, $[15, 4.4 \times 10^5]$; (c) 0.2 s, $[26.3, 1.11 \times 10^6]$; (d) 0.3 s, $[124, 2.41 \times 10^6]$; (e) 0.5 s, $[102, 7.2 \times 10^6]$; (f) 1 s, $[47.2, 1.92 \times 10^7]$; (g) 2.2 s, $[49.2, 4.51 \times 10^7]$; (h) 3.2 s, $[33.9, 5.49 \times 10^7]$.

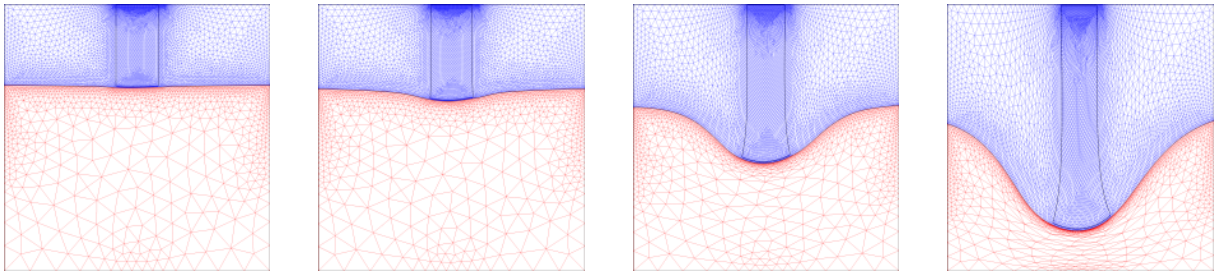

Figure 7. Mesh deformation at various time instances: (a) 0.5, (b) 1.0, (c) 2.2, (d) 3.2 s.

This statement is intended to clarify some features of the interaction of a plasma jet with a destructible surface. In contrast to the simulation of a jet of the same material, in this case a compressible gas model was used at relatively low Mach numbers ($M \leqslant 0.3$), providing a model accuracy of about 10%. In the calculation, it is also assumed that the contribution of evaporated material to the characteristics of the gas flowing at the surface is negligible.

Figure 6 shows the distribution of the heat flux along the Z axis. It can be seen that the lack of grid resolution leads to the formation of two jets at the boundary of the inlet section. Due to the relative low density of hot gas, the achievement of thermal fluxes comparable to the flow of liquid jet in a stream of nitrogen requires the implementation of much higher temperatures and speeds. One can note the change of the grid shape in adaptation region (figure 7).

The velocity field in the jet (figure 8) shows the insufficient grid resolution, that is expressed in the absence of flow in the central zone (the onset of two jets $t \approx 0.1$ s) and in the asymmetry of

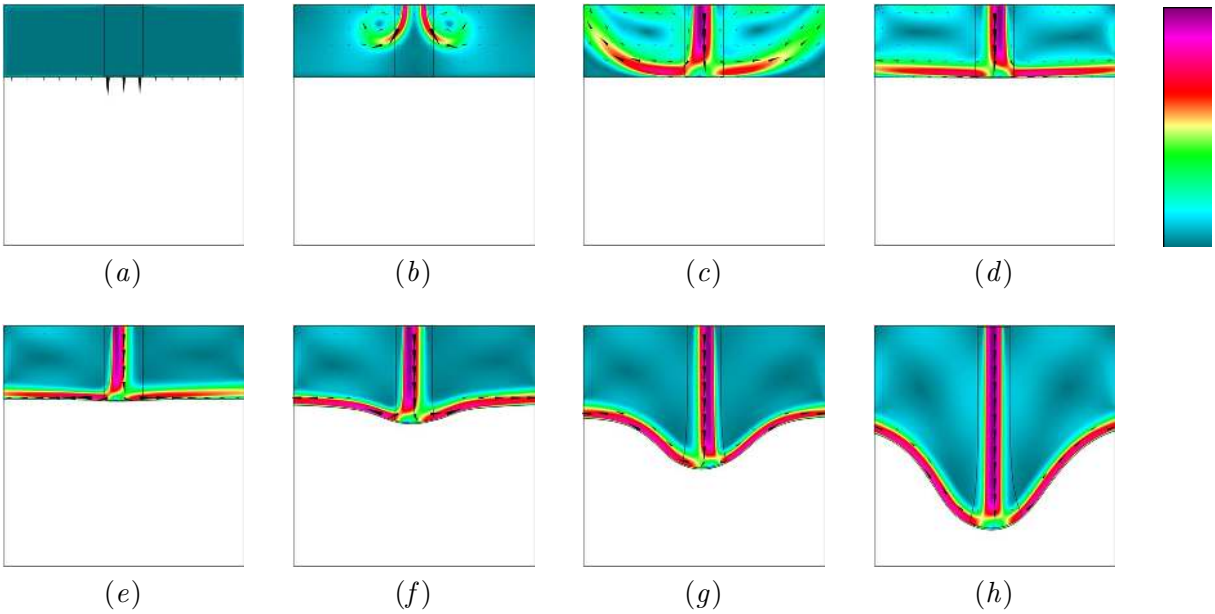

Figure 8. Speed distribution in a gas stream at different moments with the corresponding color scale ranges (m/s): (*a*) 0 s, [0, 0.185]; (*b*) 0.1 s, [0, 2.8]; (*c*) 0.2 s, [0, 5.5]; (*d*) 0.3 s, [0, 5.5]; (*e*) 0.5 s, [0, 10.7]; (*f*) 1 s, [0, 71.6]; (*g*) 2.2 s, [0, 162]; (*h*) 3.2 s, [0, 195].

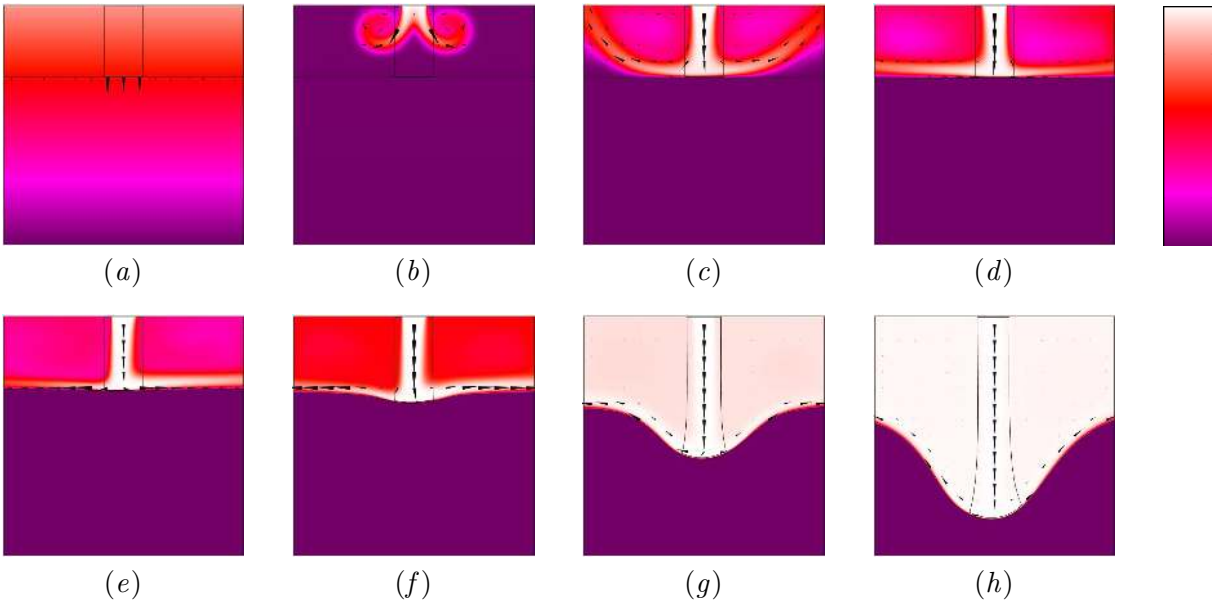

Figure 9. Temperature T distribution at different moments with the corresponding color scale ranges (K): (*a*) 0 s, [503, 509]; (*b*) 0.1 s, [503, 981]; (*c*) 0.2 s, [503, 1410]; (*d*) 0.3 s, [503, 1800]; (*e*) 0.5 s, [503, 2470]; (*f*) 1 s, [503, 3670]; (*g*) 2.2 s, [503, 4950]; (*h*) 3.2 s, [503, 5300].

velocity field in the jet ($t \approx 0.5$–2.2 s). Subsequently, the jet becomes stable. It should be noted that spreading filaments do not detach from the surface of a solid throughout the calculation.

The appearance of the cavity occurs at $t \approx 0.5$ s. Later, a heat flux (55 MW/m^2) comparable to the liquid jet is achieved.

The temperature field (figure 9) suggests that the flow evolution depends on the distance from the upper boundary of the computational domain to the interface between solid and gaseous media. Indeed, if this distance is relatively small, then the initial interaction of the hot gas and the wall is carried out by the hot "wings" of the two jets (together with the central zone), so the initial contact area is quite large (2–3 characteristic scales), and the high-speed T-shape flow is already set at the hot fluid layer. If the distance to the surface is large enough, then the two initial vortices in the induction zone of the jet are left behind and jet impinges the surface at some local area, followed by spilling over the solid. It should be noted that even at such small distances, oscillations of the jet core are observed, which lead to a shift of stagnation spot at the solid surface.

Despite the absence of intense vortices around stream, at $t \geqslant 2$ s there is a rapid warming of the entire gas region up to the jet temperature. Attention should also be paid to the process of deformation of the adapted mesh zone.

4. Conclusion

The test simulation of the problems of two-phase interaction of the immersed jet of molten liquid and hot gas, on the whole, qualitatively showed the main flow characteristics: the generation of large-scale vortices around in the induction zone, jet oscillations when it collides with an obstacle, the shape of the cavity formed. At this stage of the program testing, an important result is the similarity of the cavity profile shape during operation of a real plasma torch and the results of two-dimensional numerical simulation.

However, we note a number of serious limitations identified when using this software package:

- the impossibility of calculating the convective and diffusion mixing of two gas phases, which takes place, in particular, when a immersed stream of argon flows into the atmosphere;
- the need to allocate large amounts of memory for the algorithm to work on small grids;
- non-uniformity of the convergence process during mesh refinement;
- restriction on Mach numbers (M about 0.3) in the model for calculating a compressible gas, the absence of models for calculating transonic flows.

We emphasize that the preliminary modeling contains a number of assumptions that significantly differ from experimental conditions:

- the real interaction between the jet and solid substrate is three-dimensional;
- being heated the solid body is surrounded by a veil of decomposition products, as well as gases emanating from the pores (or dissolved) in the sample material;
- combustion (oxidation) of matter evaporating or sublimating from the sample, in particular carbon atoms and particles, occurs both when using nitrogen and argon as plasma forming gas (due to mixing and molecular diffusion);
- the sample has a finite size increasing its total temperature at sufficiently long heat exposure;
- there is a slight displacement as well as deformation and morphological transitions in the sample exposed to plasma jet.

The performed simulation of the interaction between a high-speed plasma jet and solid shows the possibility of studying a variety of occurring processes, such as heating, temperature field stabilizing, sample temperature fluctuations, its partial destruction, and also plasma chemical reactions in the interaction zone, including surface burning of sample material and its sublimate in nonequilibrium plasma flow.

Acknowledgments
The authors thank the rector of the Dagestan State University for the opportunity to use the licensed version of the COMSOL program. The present work is supported by the Russian Science Foundation (grant No. 19-49-02031).

References
[1] Reynolds W C, Parekh D E, Juvet P J D and Lee M J D 2003 *Annu. Rev. Fluid Mech.* **35** 295–315
[2] Sandham N D and Reynolds W C 1991 *J. Fluid Mech.* **224** 133–58
[3] Huerre P and Monkewitz P A 1985 *J. Fluid Mech.* **159** 151
[4] Drazin P G and Reid W H 2004 *Hydrodynamic Stability* (Cambridge University Press)
[5] Fincke J R, Crawford D M, Snyder S C, Swank W D, Haggard D C and Williamson R L 2003 *Int. J. Heat Mass Transfer* **46** 4201–13
[6] Fincke J R and Pentecost G C 1991 Laminar to turbulent transition and entrainment in thermal plasma jets *Proc. of the 28th National Heat Transfer Conf.* (American Society of Mechanical Engineers) pp 101–6
[7] Broadwell J E and Breidenthal R E 1982 *J. Fluid Mech.* **125** 397
[8] Mungal M G and Dimotakis P E 1984 *J. Fluid Mech.* **148** 349–82
[9] Dimotakis P E 1986 *AIAA J.* **24** 1791–6
[10] Brown G L and Roshko A 1974 *J. Fluid Mech.* **64** 775–816
[11] Ricou F P and Spalding D B 1961 *J. Fluid Mech.* **11** 21–32
[12] Abramovich B N, Yakovlevsky O V, Smirnova I P, Secundov A N and Krashensnnikov S Y 1969 *Astronaut. Acta* **14** 911–6
[13] Monkewitz P A and Sohn K D 1988 *AIAA J.* **26** 911–6
[14] Russ S and Strykowski P J 1993 *Phys. Fluids A* **5** 3216–25
[15] Lepicovsky J 1990 *AIAA J.* **28** 478–82
[16] Fincke J R, Swank W D, Snyder S C and Haggard D C 1993 *Rev. Sci. Instrum.* **64** 3585–93
[17] Dimotakis P E 2000 *J. Fluid Mech.* **409** 69–98
[18] Belevtsev A A, Kavyrshin D I, Sargsyan M A, Chinnov V F, Efimov A V and Shcherbakov V V 2018 *J. Phys. D: Appl. Phys.* **51** 484002
[19] Chinnov V F, Sargsyan M A, Gadzhiev M K, Khromov M A, Kavyrshin D I and Chistolinov A V 2018 *J. Phys.: Conf. Ser.* **946** 012174
[20] Sargsyan M A, Chinnov V F, Kavyrshin D I, Gadzhiev M K, Khromov M A, Chistolinov A V and Senchenko V N 2017 *J. Phys.: Conf. Ser.* **891** 012313
[21] Tyuftyaev A S, Gadzhiev M K, Sargsyan M A, Chinnov V F, Demirov N A, Kavyrshin D I, Ageev A G and Khromov M A 2016 *J. Phys.: Conf. Ser.* **774** 012204
[22] Chinnov V F, Tyuftyaev A S, Kavyrshin D I, Ageev A G, Sargsyan M A and Gadzhiev M K 2018 *High Temp.* **56** 25–32
[23] Ageev A G, Kavyrshin D I, Sargsyan M A, Gadzhiev M K and Chinnov V F 2017 *Int. J. Heat Mass Transfer* **107** 146–53
[24] Isakaev E K, Sinkevich O A, Tyuftyaev A S and Chinnov V F 2010 *High Temp.* **48** 97–125
[25] Wolff F and Viskanta R 1988 *Int. J. Heat Mass Transfer* **31** 1735–44
[26] Alexiades V, Hannoun N and Mai T Z 2003 Tin melting: Effect of grid size and scheme on the numerical solution *Proc. of the 5th Mississippi State Conf. on Differential Equations and Computational Simulations* pp 55–69